Research Article | Vol. 9, No. 10 | 1 Oct 2018 | BIOMEDICAL OPTICS EXPRESS 4988
Biomedical Optics EXPRESS

Superhydrophobic silver film as a SERS substrate for the detection of uric acid and creatinine

YUDONG LU,[1] CHANGJI WU,[1] RUIYUN YOU,[1,*] YANG WU,[1] HUIYING SHEN,[1] LANJIN ZHU,[1] AND SHANGYUAN FENG[2]

[1]*College of Chemistry and Materials Science, Fujian Key Laboratory of Polymer Materials, Fujian Normal University, Fuzhou, Fujian 350007, China*
[2]*Key Laboratory of Optoelectronic Science and Technology for Medicine of Ministry of Education, Fujian Provincial Key Laboratory of Photonics Technology, Fujian Normal University, Fuzhou 350007, China*
**youruiyun@fjnu.edu.cn*

Abstract: Superhydrophobic silver films were fabricated by silver-mirror reaction and surface functionalization with thiol. The thiol-functionalization significantly improved the hydrophobic property of the Ag films (AFS), and their contact angle values slightly increased with the extension of a thiol alkyl chain, reaching about 160°. The surface-enhanced Raman scattering (SERS) detection capacity of these films were investigated, and AFS-Dodec showed the best substrate for R6G molecule detection with the concentration limit of 10^{-11} M. AFS functionalized with dodecanethiol (AFS-Dodec) was applied for the SERS detection of uric acid and creatinine, it exhibited good linear dependence relationship between the Raman intensity and analyte concentration in the concentration range of 5~1000 μM.

1. Introduction

Uric acid is a metabolite considered as an inert end-product of purine catabolism, its concentration in blood is determined by the balance between uric acid production and excretion. It is identified as an important biomarker in urine and serum samples for metabolism abnormally, strong correlated of renal dysfunction in rheumatoid arthritis cardiovascular [1,2] and gout disease [3]. The high concentration of uric acid (>0.4 mM) is associated with patients experiencing severe preeclampsia [4]. Likewise, creatinine in serum also reflects the extent of kidney damage, such as acute kidney injury [5]. Therefore, an effective detection method is imperative for monitoring the content and change.

Surface-enhanced Raman scattering (SERS) [6,7] is a sensitive spectroscopic technique capable of providing a characteristic molecular vibrational fingerprint, even at trace concentrations. Since the first report on SERS in 1977, many efforts have been made to achieve higher sensitivity in chemical and biological detection [8,9]. It is generally regarded that SERS enhancement stems from two mechanism [10,11]: One is chemical enhancement, which is realized by charge transfer between the analytes and the SERS substrate; the other is electromagnetic enhancement, which plays the dominant role in SERS enhancement [12,13]. It is well known that metal nanoparticles such as silver and gold can lead to strong electromagnetic fields, which is termed "hot spot" in SERS measurements [14], thus nanostructured metal material with different morphologies (nanorod, nanosphere, nanocubic, nanowire, *etc*) were fabricated to create more hot spots [15]. In addition to the intrinsic hotspot density, the surface state of the SERS substrates also considerably influences the SERS effect. The common SERS substrates have hydrophilic surface, which makes the analyte solution spread over the whole surface, resulting in the low detection limit even with high density-hotspots. Interestingly, the hydrophobic substrate can cause great shrinkage of the solution during the solvent evaporation process, and the analyte molecules are

#340599 https://doi.org/10.1364/BOE.9.004988
Journal © 2018 Received 25 Jul 2018; revised 14 Sep 2018; accepted 14 Sep 2018; published 24 Sep 2018

Biomedical Optics EXPRESS

concentrated to a smaller size and increase their density, which enables more analyte molecules to be exposed to laser spot, resulting in high detection selectivity.

The hydrophobic property of the substrate is often affected by two factors: one is the chemical composition of the surface. Sun used two different chemical compositions to prepare hydrophilic and hydrophobic platforms that resulted in approximately perpendicular contact angles with 30° and 110° [16]. The other is hierarchical surface structure; the micro/nano surface structure can retain more air and form an air layer, implying that fluids cannot wet the inner structure. Safaee [17] studied the hydrophobic properties of rough and smooth silver film under the same conditions, and found that the rough surface acquired a better water contact than the smooth one. Huang [18] reported that Taro-leaf@Ag showed great enhancement of Raman signal due to the taro leaf's super-hydrophobic property.

Because sulfhydryl group easily binds to the heavy metal, SERS substrates based on heavy metal can be decorated with thiol compound to modulate their surface state, with the purpose of high SERS detection sensitivity. Different thiols (Decanethiol [19], 1-dodecanethiol [20] and (1-mercaptoundeca-11-yl) tri-(ethylene glycol) [20]) have been used to improve the adsorption of glucose molecules onto bare silver surfaces. Liu [20] fabricated oxidizing nano-sized Cu films and used octadecanethiol modification to prepare super-hydrophobic material. Herein, we prepared hydrophobic substrates by modifying the surface of silver film with different thiols (Fig. 1). Owing to the superhydrophobic properties of the obtained silver film, the mixed droplets of the analyte molecules and Ag colloid suspension evaporated to form condensed "hot spots", thus efficient surface-enhanced Raman spectroscopy detection was achieved on the superhydrophobic silver film.

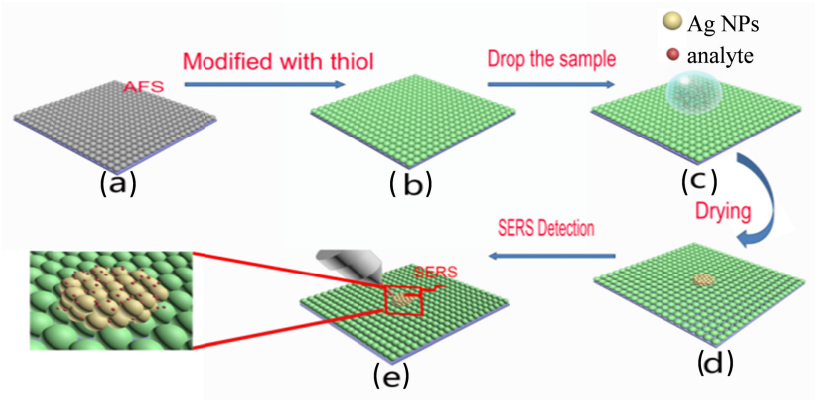

Fig. 1. Schematic illustration of the synthetic process for superhydrophobic silver film and the detection spot of the mixture of analyte and Ag nanoparticles formed on the substrate for SERS measurement.

2. Experiment

2.1 Materials

All reagents used were of analytical grade, and the solutions were prepared with Millipore water. Silver nitrate (purity≥99.8%), glucose, ammonium hydroxide, hydroxylammonium chloride, butanethiol, hexanethiol, heptanethiol, octanethiol, decanethiol,1-dodecanethiol, and octadecanethiol were purchased from Guangdong Weng Jiang Chemical Reagent Co.,Ltd. Crystal violet and malachite green were obtained from Sinopharm .Uric acid (99%) was purchased from MAKLIN and creatinine (99%) was from Aladdin.

2.2 Fabrication of the platform

Ag film (AFS) was fabricated by using the silver mirror reaction. Typically, aqua ammonia was added to 30 mL 2 wt% $AgNO_3$ solution to form Tollens' reagent in a 50 mL centrifuge

Biomedical Optics EXPRESS

tube. Thereafter, 1 mL 6% glucose solution was added to the mixture as a reducing reagent. The glass slides (25 mm × 75 mm) were sonicated in acetone, ethanol, and ultrapure water for 10 min respectively, to remove organic contaminants. The clean glass slide was put into the prepared mixture and kept in water bath at 75°C for 15 min.

The obtained AFS was immersed in 30 mL thiol ethanol solution, which was dissolved (butanethiol, hexanethiol, heptanethiol, octanethiol, decanethiol, 1-dodecanethiol or octadecanethiol) with ethyl alcohol for self-assembly for saturated adsorption. After keeping in the thiol ethanol solution for 12 h, the film was taken out and rinsed with ethanol. The obtained Ag film was denoted as AFS-*x* (*x* is the prefix of thiol)

2.3 *Synthesis of Ag colloid*

90 mL$AgNO_3$ aqueous solution (1mM) was added to the conical flask, then 4.5 mL of 0.1 M aqueous NaOH and 4.5 mL of 0.06 M hydroxyl ammonium chloride were mixed by shaking and added to the conical flask while being stirred constantly for 10 min. The obtained Ag colloid was greyish-green and an absorption peak was at about 440nm (Fig. 2(a)). The silver nanoparticles were spherical with particle size of 20~80 nm (Fig. 2(b)).

1.5 mL Ag colloid was added into a centrifuge tube, and put it in the high speed centrifuge (TGL-18C) with 10000 rpm/min for 10 min. Then the supernatant was removed, leaving 6 μL of concentrated silver colloid for future use.

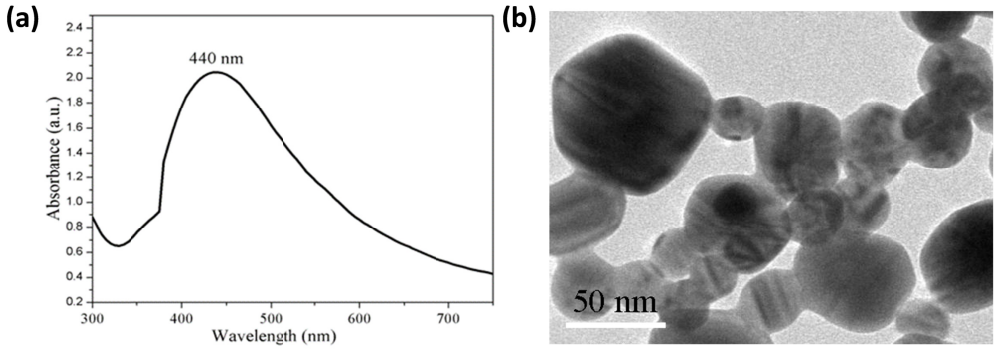

Fig. 2. (a) UV-Vis absorption spectrum of Ag colloid; **(b)** TEM of the Ag Nps.

2.4 *Sample preparation*

2 μL concentrated Ag colloid and 5 μL analyte solution were mixed in a 0.5 mL centrifuge tube. Then, pipetted all of suspension and dropped onto the Ag film surface. Finally, SERS detection was carried out once the spot was dried.

2.5 *Characterization and SERS detection*

The absorption spectrum of Ag colloid was examined by UV1902 UV-Vis spectrometer (Lengguang Tech., Shanghai, China). The surface structure of the Ag film was examined by JSM-6380LV scanning electron microscope (SEM) (JEOL Ltd, Japan). FTIR-ATR spectra were obtained on a Nicolet Magna 670 fourier transform infrared spectrometer (Thermo Nicolet Corporation, America). The static contact angle was tested with Bruks DSA25static contact angle meter (KRüSS Ltd, Germany). SERS measurement was performed on a Renishaw confocal Raman instrument (Renishaw, Britain) equipped with a 785 nm wavelength laser and 20 × objective. The laser power was set at 0.66 mW, and the integration time of the Raman spectrum was 10 s.

Biomedical Optics EXPRESS

3. Results

As shown in Fig. 2(a), the AFS consists of the silver particles with the size ranging from 50 to 500 nm. The particles randomly aggregate together, forming a multi-scale and rough surface structure. It can be seen from the inset in Fig. 3(a), AFS shows hydrophobic behavior with the water contact angle (WCA) of 102.6 °, which is much higher than that of a commercial Ag foil (64°). This could be due to the different surface roughness between AFS and Ag foil (Fig. 3(b)). Chemically modification is an effective way to prepare hydrophobic surfaces, thus AFS was functionalized with a series of organic thiols to improve its hydrophobic property. In the case of AFS-Dodec, the discharge behavior is obviously observed and the Ag particles' morphology becomes fuzzy in the SEM image (Fig. 3(c)), this could be attributed to the low conductivity of thiol bonded to Ag particles.

To confirm the existence of thiol in the film, FTIR-ATR spectrum of AFS-Dodec was carried out, with AFS as a control. As shown in Fig. 4, AFS-Dodec presents the characteristic bands {2851 cm^{-1} (v_s-CH_2); 2921 cm^{-1} (v_{as}-CH_2); 1464 cm^{-1} (δ-CH_2); 720 cm^{-1}(δ-CH_2) for dodecanethiol. It is noted that the CH_2 symmetric and antisymmetric stretching bands has a red shift compared to those of pristine dodecanethiol (2854 and 2925 cm^{-1}), this suggests that dodecanethiol is bound to the silver metallic surface [20]. All these results indicate that AFS was successfully modified with thiol. As expected, AFS-Dodec surface was transformed into superhydrophobic with the WCA of 157° (Fig. 3(c)).

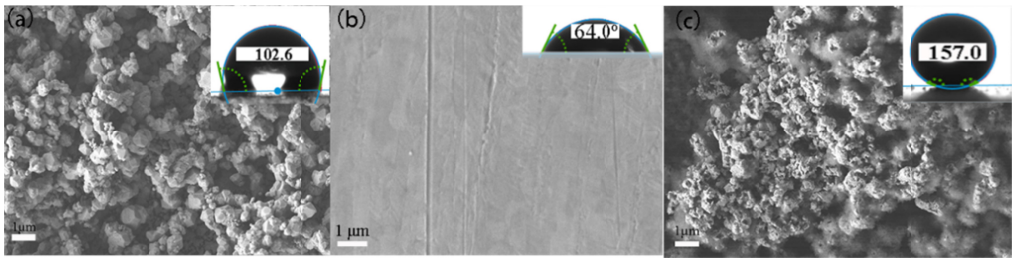

Fig. 3. SEM images of AFS (a), commercial Ag foil (b) and AFS-Dodec (c); the inset is the optical image of the water droplet on the substrate.

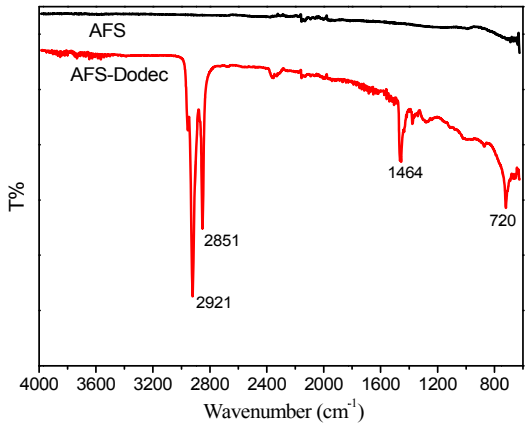

Fig. 4. FTIR-ATR spectra of AFS and AFS-Dodec.

We also measured the WCA of the silver film modified with other thiols as shown in Fig. 5(a). The contact angle value slightly increases with the extension of a thiol alkyl chain, reaching about 150°, this implies that the thiol-modifed silver films have superhydrophobic surface. To demonstrate the condensation effect on the superhydrophobic surface, a 12μL

Biomedical Optics EXPRESS

suspension liquid was dropped onto AFS-Dodec and the change of the droplet on the substrate was recorded during natural evaporation. As shown in Fig. 5(b), the spot size is almost unchanged on AFS, but the spot diameter decreases from 3 mm to 1 mm on AFS-Dodec; thus the spot area of AFS-Dodec is only 1/9 of that of AFS. The generated spot with smaller size definitely concentrate the analyte concentration, which could improve the detection sensitivity for SERS measurement.

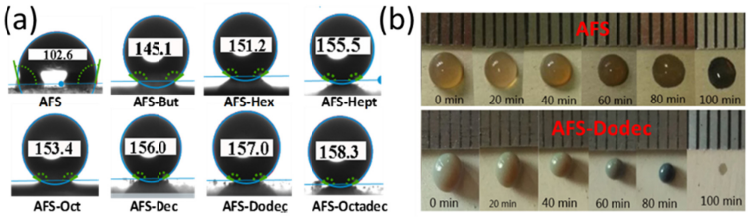

Fig. 5. (a) Optical images of water droplet on the AFS modified with different thiols, (b) Images of the time-evolution of a droplet on AFS and AFS-Dodec during natural evaporation.

As displayed in Fig. 6(a), R6G was used as a probe molecule for SERS measurement over AFS with/without thiol modification. All samples clearly exhibit characteristic bands of R6G at 1182 cm^{-1}, 1310 cm^{-1}, 1362 cm^{-1} and 1508 cm^{-1} [21].The signal intensity in the spectra increases with the increase in carbon chain length of thiol, the strongest signal is obtained over AFS-Dodec. This might be because the increasing carbon chain can offer an optimal "gap" between Ag NPs and AFS. However, when the chain increases to 18 carbons, their gap is too wide to enhance the intensity. Therefore, dodecanethiol is the best choice to modify AFS for SERS measurement. For demonstrating the impact of "gap" between AFS and Ag NPs, experiment was conducted by comparing the detection limit Ag NPs on glass and AFS. The detection limit was low with 10^{-8} M R6G (Fig. 6(b)) on glass and more obvious with 10^{-9} M R6G (Fig. 6(c)) on AFS. Further, we also measured the Raman spectra of the AFS-Dodec substrate with variable R6G concentration ranging from 10^{-8} to 10^{-11} M. As displayed in Fig. 7(a), the intensity of characteristic Raman peak decreases with the decrease in the concentration of the proved R6G. Figure 7(b) shows the linear dependence relationship of Raman intensity of the peak at 1501 cm^{-1} and the concentration of R6G. This linear proportional relation implies that the SERS substrate has a potential about the SERS sensitivity for low concentration and ability for the quantitative analysis.

Biomedical Optics EXPRESS

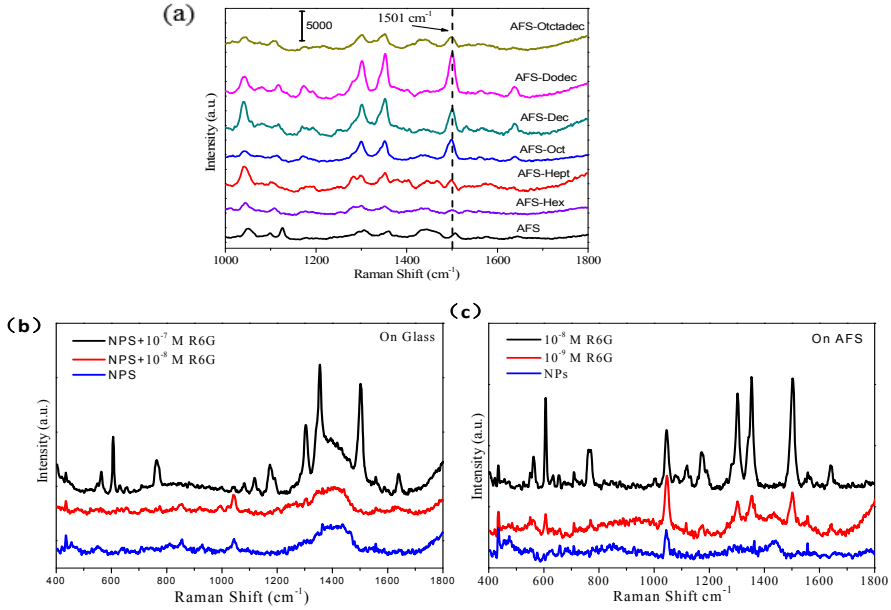

Fig. 6. (a) SERS spectra of 10^{-9} M R6G mixed with Ag colloid over AFS modified with different thiols. (b) Detection of R6G with R6G on glass. (c) Detection of R6G with R6G on AFS.

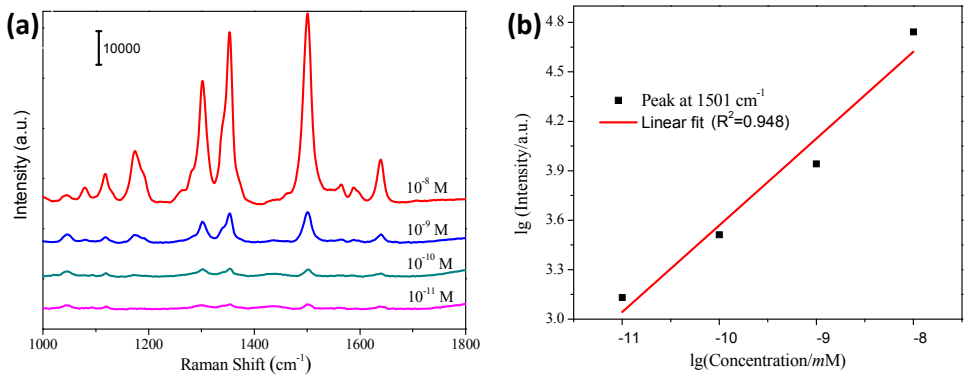

Fig. 7. (a) SERS spectra obtained from 10^{-8}~10^{-12} M R6G mixed with Ag colloid on AFS-Dodec, (b) the plots for SERS peak intensity at 1501 cm^{-1} as a function of R6G concentration

To investigate the practical application of this superhydrophobic silver film, AFS-Dodec was used as SERS substrate to detect uric acid and creatinine. In the case of uric acid (shown in Fig. 8(a), all samples display strong Raman peaks at 638, 811, 885, 1133, 1389 and 1608 cm^{-1}. The 638 cm^{-1} belongs to skeletal ring deformation and 1133 cm^{-1} is originated from C-N, more details are shown in Table 1. It is noted that SERS can equally occur for all type of molecules in a bioprobe and the appropriate select of the target Raman lines can increase signal-to-noise ratio [22–24], thus the peak at 1133 cm^{-1} was selected for further analysis of uric acid. Figure 8(b) presents the linear dependence relationship between Raman intensity of the peak at 1133 cm^{-1} and the concentration of uric acid, with $R^2 = 0.996$. Similar result was obtained for creatinine detection, shown in Fig. 9. The characteristic Raman peaks intensity increases with the increase in the concentration of creatinine, and the linear dependence relationship between Raman intensity of the peak at 681 cm^{-1} and the concentration of

Biomedical Optics EXPRESS

creatinine is achieved in the range of 5-1000 μM. The results indicate that the fabricated superhydrophobic silver film could be used as SERS substrate for practical detection of uric acid and creatinine.

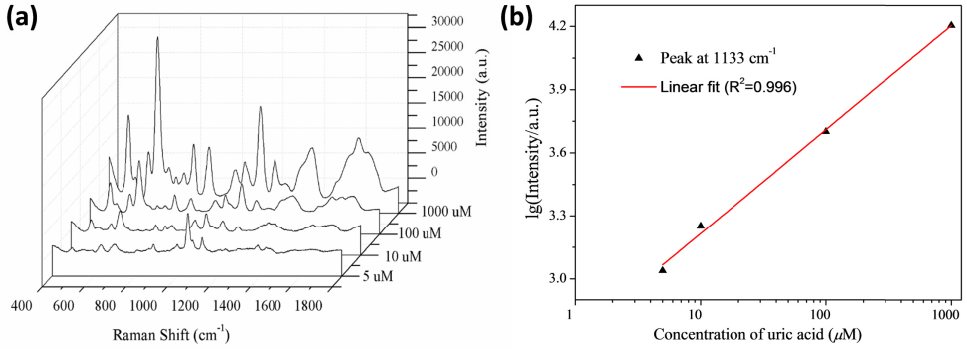

Fig. 8. (a) SERS spectra obtained from 5~1000 μM uric acid mixed with Ag colloid on AFS-Dodec;(b) the plots for SERS peak intensity at 1133 cm^{-1} as a function of creatinine concentration

Table 1. Band assignment for uric acid and creatinine

Uric Acid [25,26]			**Creatinine** [27,28]		
Experimental SERS mode (cm^{-1})	SERS mode in reference	Assignment	Experimental SERS mode (cm^{-1})	SERS mode in reference	Assignment
497	508	C-N-C ring vibration	576	550	C-N bending /ip ring deformation
594	601	oop NH bending/oop ring deformation	614	640	Skeletal ring deformation
638	640	Skeletal ring deformation	681	680	In-plane ring scissoring/C-NH_2 stretching/ring stretching
764	764	oop NH bending/oop ring deformation	840	812	Ring vibration
811	812	Ring vibration	915	940	C-N stretching
885	889	N-H bending	1046	1017	Ring vibration
1012	1017	Ring vibration	1337		
1057	1074	C-Nstretching/OH bending/mixed	1421		
1133	1134	C-N	1754	1752	C = O stretching/N-H inplane bending/NH2 wagging
1204	1206	N-C-C stretching and bending			
1389	1369	C-O			
1608	1607	C = O stretching			

Biomedical Optics EXPRESS

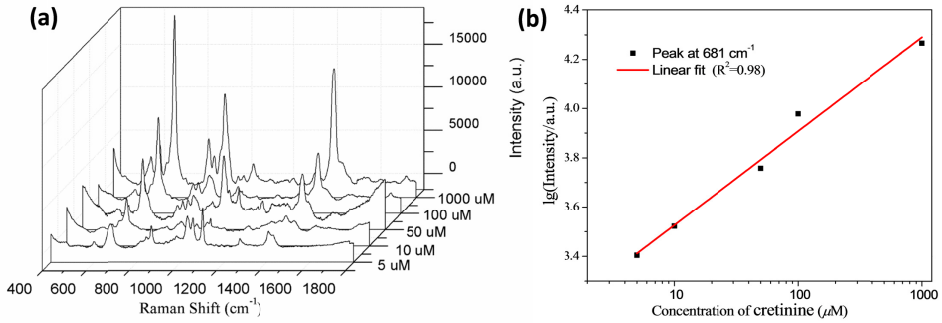

Fig. 9. (a) SERS spectra obtained from 5~1000 μM creatinine mixed with Ag colloid on AFS-Dodec; (b) the plots for SERS peak intensity at 681 cm^{-1} as a function of creatinine concentration

4. Discussion

The hydrophobic behavior of AFS, compared to Ag foil, is closely related to the microstructure with hierarchical structure that produce a capillary force at the liquid-air interface inside the indentions, which prevents liquid from entering them [29–31], endowing it with hydrophobic property. After functionalized with thiols, the condensation effect was observed in the samples with CA >150° (AFS-Hex, AFS-Hept, AFS-Oct, AFS-Dec, AFS-Dodec and AFS-Octadec) when compared to the unmodified AFS. Such effect could contribute to the enhancement of SERS over the modified sample. However, the modified samples displayed different SERS signal intensities in the spectra (showed in the Fig. 6(a)). This means that the greatest SERS performance over AFS-Dodec (the performance has been checked many times) is not just due to "the condensation effect". And as the Fig. 6(b) and 6(c) showed, the difference of detection limit of R6G on glass and AFS (10^{-8} M on glass and 10^{-9} M on AFS) revealed the enhancement effect between AFS and Ag NPS. It may be worked with AFS or the gap between AFS and Ag NPS. Moreover, the contacted rough things (AFS and Ag NPS) must exist crevice. Combining the different carbon chains of the thiols used in this study which obtained different SERS signal intensities in the spectra, we regarded carbon chains might be another important influence factor to the gap size between Ag NPs and AFS. Of course, more insightful work is needed to reveal the mechanism for the enhanced SERS performance in future work.

Many biomolecules are highly important to disease diagnosis. And owing to the sensitive and rapid detection of SERS, it has been widely used in bio-areas [32–34] and discovered potential biomedical applications. But most biomolecules are low content and have the characteristic of relatively low Raman scattering cross section. Therefore, labeled with a probe with strong SERS signal is a good method to make it out [35]. But label-free SERS detection can provide the fingerprint information on biomolecules directly related to their structure in simpler and more cost-effective way. Compared with ordinary dripping and dry test, the condensation effect on superhydrophobic-AFS would concentrate the biomolecules and increase the sensitive, like 5 μM uric acid in this work but 186 μM in previous one [25]. And it takes a short time with 1 min instead of 140 min by HPLC [25]. The superiority of sensitivity, low detection limit, rapid of SERS could play an important role in biomolecules for disease diagnosis, and the condensation effect adds wings.

5. Conclusion

The superhydrophobic silver films (AFS) were successfully fabricated by silver-mirror reaction and surface functionalization with thiols. It was found the obtained silver film has a

Biomedical Optics EXPRESS

rough surface, and the surface becomes superhydrophobic after thiol-functionalization. By virtue of the condensation effect on the superhydrophobic surface, the silver film modified with dodecanethiol behaves as the best SERS substrate for the detection of R6G molecule with the detection limit of 10^{-11} M. AFS-Dode was also applied for the detection of uric acid and creatinine, and it exhibited linear dependence relationship between Raman peak intensity and the analyte concentration range of 5~1000 μM. The study demonstrated a facile strategy to fabricate efficient SERS sensor with high detection sensitivity.

Funding

National Natural Science Foundation of China (Nos. 61575043); Natural Science Foundation of Fujian Province of China (grant no. 2016J01292); Program for New Century Excellent Talent in Fujian Province (Nos. J1-1160).

Acknowledgment

This work was supported by Center of Engineering Technology Research for Microalgae Germ plasma Improvement of Fujian, Southern Institute of Oceanography, Fujian Normal University, Fuzhou, China, 350117.

Disclosures

The authors declare that there are no conflicts of interest related to this article.

References and links

1. V. F. Panoulas, H. J. Milionis, K. M. J. Douglas, P. Nightingale, M. D. Kita, R. Klocke, M. S. Elisaf, and G. D. Kitas, "Association of serum uric acid with cardiovascular disease in rheumatoid arthritis," Rheumatology (Oxford) **46**(9), 1466–1470 (2007).
2. C. Borghi, E. A. Rosei, T. Bardin, J. Dawson, A. Dominiczak, J. T. Kielstein, A. J. Manolis, F. Perez-Ruiz, and G. Mancia, "Serum uric acid and the risk of cardiovascular and renal disease," J. Hypertens. **33**(9), 1729–1741 (2015).
3. S. Liu, F. Perez-Ruiz, and J. N. Miner, "Patients with gout differ from healthy subjects in renal response to changes in serum uric acid," Joint Bone Spine **84**(2), 183–188 (2017).
4. C. S. Buhimschi, E. R. Norwitz, E. Funai, S. Richman, S. Guller, C. J. Lockwood, and I. A. Buhimschi, "Urinary angiogenic factors cluster hypertensive disorders and identify women with severe preeclampsia," Am. J. Obstet. Gynecol. **192**(3), 734–741 (2005).
5. E. J. Erlandsen and E. Randers, "Reference intervals for plasma cystatin C and plasma creatinine in adults using methods traceable to international calibrators and reference methods," J. Clin. Lab. Anal. **32**(6), e22433 (2018).
6. K. Kneipp, H. Kneipp, and, H. G. Bohr, *Single-Molecule SERS Spectroscopy* (Springer, 2006), pp. 261–277.
7. K. Kneipp, H. Kneipp, I. Itzkan, R. R. Dasari, and M. S. Feld, "Surface-enhanced Raman scattering and biophysics," J. Phys. Condens. Matter **14**(18), R597–R624 (2002).
8. J. A. Kellum, F. E. Sileanu, R. Murugan, N. Lucko, A. D. Shaw, and G. Clermont, "Classifying AKI by Urine Output versus Serum Creatinine Level," J. Am. Soc. Nephrol. **26**(9), 2231–2238 (2015).
9. E. Cepeda-Pérez, T. López-Luke, P. Salas, G. Plascencia-Villa, A. Ponce, J. Vivero-Escoto, M. José-Yacamán, and E. de la Rosa, "SERS-active Au/SiO_2 clouds in powder for rapid ex vivo breast adenocarcinoma diagnosis," Biomed. Opt. Express **7**(6), 2407–2418 (2016).
10. T. Gong, K. V. Kong, D. Goh, M. Olivo, and K. T. Yong, "Sensitive surface enhanced Raman scattering multiplexed detection of matrix metalloproteinase 2 and 7 cancer markers," Biomed. Opt. Express **6**(6), 2076–2087 (2015).
11. L. Xia, M. Chen, X. Zhao, Z. Zhang, J. Xia, H. Xu, and M. Sun, "Visualized method of chemical enhancement mechanism on SERS and TERS," J. Raman Spectrosc. **45**(7), 533–540 (2014).
12. A. Otto, "The 'chemical' (electronic) contribution to surface-enhanced Raman scattering," J. Raman Spectrosc. **36**(6-7), 497–509 (2005).
13. E. C. L. Ru, M. Meyer, E. Blackie, and, P. G. Etchegoin, "Advanced aspects of electromagnetic SERS enhancement factors at a hot spot," J. Raman Spectrosc. **39**, 1127–1134 (2010).
14. S. V. Gaponenkoa and D. V. Guzatovb, "Possible rationale for ultimate enhancement factor in single molecule Raman spectroscopy," Chem. Phys. Lett. **477**(4-6), 411–414 (2009).
15. S. L. Kleinman, R. R. Frontiera, A. I. Henry, J. A. Dieringer, and R. P. Van Duyne, "Creating, characterizing, and controlling chemistry with SERS hot spots," Phys. Chem. Chem. Phys. **15**(1), 21–36 (2013).
16. Y. Sun, Z. Han, H. Liu, S. He, L. Yang, and J. Liu, "Three-dimensional hotspots in evaporating nanoparticle sols for ultrahigh Raman scattering: solid-liquid interface effects," Nanoscale **7**(15), 6619–6626 (2015).

Biomedical Optics EXPRESS

17. A. Safaee, D. K. Sarkar, and M. Farzaneh, "Superhydrophobic properties of silver-coated films on copper surface by galvanic exchange reaction," Appl. Surf. Sci. **254**(8), 2493–2498 (2008).
18. J. A. Huang, Y. L. Zhang, Y. Zhao, X. L. Zhang, M. L. Sun, and W. Zhang, "Superhydrophobic SERS chip based on a Ag coated natural taro-leaf," Nanoscale **8**(22), 11487–11493 (2016).
19. K. E. Shafer-Peltier, C. L. Haynes, M. R. Glucksberg, and R. P. Van Duyne, "Toward a glucose biosensor based on surface-enhanced Raman scattering," J. Am. Chem. Soc. **125**(2), 588–593 (2003).
20. C. Zhu, G. Meng, Q. Huang, Z. Huang, and Z. Chu, "Au hierarchical micro/nanotower arrays and their improved SERS effect by Ag nanoparticle decoration," Cryst. Growth Des. **11**(3), 748–752 (2011).
21. S. W. Han, Y. Kim, and K. Kim, "Dodecanethiol-derivatized Au/Ag bimetallic nanoparticles: TEM, UV/VIS, XPS, and FTIR Analysis," J. Colloid Interface Sci. **208**(1), 272–278 (1998).
22. K. A. Mahmoud and M. Zourob, "Fe3O4/Au nanoparticles/lignin modified microspheres as effectual surface enhanced Raman scattering (SERS) substrates for highly selective and sensitive detection of 2,4,6-trinitrotoluene (TNT)," Analyst (Lond.) **138**(9), 2712–2719 (2013).
23. A. Y. Panarin, I. A. Khodasevich, O. L. Gladkova, and S. N. Terekhov, "Determination of Antimony by Surface-Enhanced Raman Spectroscopy," Appl. Spectrosc. **68**(3), 297–306 (2014).
24. O. S. Kulakovich, E. V. Shabunya-Klyachkovskaya, A. S. Matsukovich, K. Rasool, K. A. Mahmoud, and S. V. Gaponenko, "Nanoplasmonic Raman detection of bromate in water," Opt. Express **24**(2), A174–A179 (2016).
25. C. Westley, Y. Xu, B. Thilaganathan, A. J. Carnell, N. J. Turner, and R. Goodacre, "Absolute quantification of uric acid in human urine using surface enhanced Raman Scattering with the standard addition method," Anal. Chem. **89**(4), 2472–2477 (2017).
26. M. Pucetaite, M. Velicka, J. Pilipavicius, A. Beganskiene, J. Ceponkusa, and V. Sablinskas, "Uric acid detection by means of SERS spectroscopy on dried Ag colloidal drops," J. Raman Spectrosc. **47**(6), 681–686 (2016).
27. M. Li, Y. Du, F. Zhao, J. Zeng, C. Mohan, and W. C. Shih, "Reagent- and separation-free measurements of urine creatinine concentration using stamping surface enhanced Raman scattering (S-SERS)," Biomed. Opt. Express **6**(3), 849–858 (2015).
28. H. Zhang, G. Li, S. Li, L. Xu, Y. Tian, A. Jiao, X. Liu, F. Chen, and M. Chen, "Boron nitride/gold nanocomposites for crystal violet and creatinine detection by surface-enhanced Raman spectroscopy," Appl. Surf. Sci. **457**, 684–694 (2018).
29. C. R. Yonzon, C. L. Haynes, X. Zhang, J. T. Walsh, Jr., and R. P. Van Duyne, "A glucose biosensor based on surface-enhanced Raman scattering: improved partition layer, temporal stability, reversibility, and resistance to serum protein interference," Anal. Chem. **76**(1), 78–85 (2004).
30. S. Shin, J. Lee, S. Lee, H. Kim, J. Seo, D. Kim, J. Hong, S. Lee, and T. Lee, "A Droplet-based high-throughput SERS platform on a droplet-guiding-track-engraved superhydrophobic substrate," Small **13**(7), 1602865 (2017).
31. L. Cao, T. P. Price, M. Weiss, and D. Gao, "Super water- and oil-repellent surfaces on intrinsically hydrophilic and oleophilic porous silicon films," Langmuir **24**(5), 1640–1643 (2008).
32. S. F. Kingsmore, "Multiplexed protein measurement: technologies and applications of protein and antibody arrays," Nat. Rev. Drug Discov. **5**(4), 310–321 (2006).
33. J. M. Yuen, N. C. Shah, J. T. Walsh, Jr., M. R. Glucksberg, and R. P. Van Duyne, "Transcutaneous glucose sensing by surface-enhanced spatially offset Raman spectroscopy in a rat model," Anal. Chem. **82**(20), 8382–8385 (2010).
34. J. Su, D. Wang, L. Nörbel, J. Shen, Z. Zhao, Y. Dou, T. Peng, J. Shi, S. Mathur, C. Fan, and S. Song, "Multicolor gold-silver nano-mushrooms as ready-to-use SERS probes for ultrasensitive and multiplex DNA/miRNA detection," Anal. Chem. **89**(4), 2531–2538 (2017).
35. M. M. Harper, B. Robertson, A. Ricketts, and K. Faulds, "Specific detection of DNA through coupling of a TaqMan assay with surface enhanced Raman scattering (SERS)," Chem. Commun. (Camb.) **48**(75), 9412–9414 (2012).